Rend. Fis. Acc. Lincei
DOI 10.1007/s12210-014-0303-3

Multi-proxy analysis in defining sedimentary processes in very recent prodelta deposits: the Northern Phlegraean offshore example (Eastern Tyrrhenian Margin)

Marina Iorio · Giovanna Capretto · Emanuela Petruccione · Ennio Marsella · Gemma Aiello · Maria Rosaria Senatore

Received: 27 March 2013 / Accepted: 24 March 2014

Abstract A multi-proxy analysis of Volturno River prodelta deposits in the outer shelf of Northern Phlegraean margin (Eastern Tyrrhenian Sea) has been carried out to reconstruct the sedimentary processes acting during recent times. The late Holocene sediments were characterized through Subbottom Chirp profiles coupled with sedimentological and petrophysical data. The chronostratigraphic framework was achieved by means of colorimetric parameter a^* correlations with nearby dated marine sediment. A time interpretation of about 2,300 years BP is estimated for the sedimentary record collected in the cores. Seismic stratigraphic analysis shows late Holocene outer shelf deposits, characterized by fluid escape features and small-offset faults. However, the undisturbed sedimentation and the preservation of an internal geometry at decimetre scale, as detected by the sedimentological and petrophysical analysis, indicates a slow sliding without sediment reworking for this sedimentological body. So far a possible recent (<2,300 years BP) shear dominated downward displacement of high water content sediments, triggered by the occurrence of seismic activity, is inferred. Based on the depth-age conversion of the detected lithological features, a regular climatically driven change in the sediment supply of the prodelta depositional environment is suggested. The detection of spectrophotometry correlations of Holocene shelf margin sediments, several km apart, goes beyond the previous work and confirms even for continental shelf area the potential value of spectrophotometer data in high-resolution stratigraphic correlations.

Keywords Multi-proxy analysis · Highstand prodelta sediments · Spectroscopy · Very high frequency climatic change

M. Iorio (✉) · E. Petruccione · E. Marsella · G. Aiello
Istituto per l'Ambiente Marino Costiero (IAMC), Consiglio Nazionale delle Ricerche (CNR), Calata Porta di Massa, Porto di Napoli, 80133 Naples, Italy
e-mail: marina.iorio@iamc.cnr.it

G. Capretto · M. R. Senatore
Dipartimento di Scienze per la Biologia, la Geologia e l'Ambiente, Università degli Studi del Sannio, Via dei Mulini 59/A, 82100 Benevento, Italy

1 Introduction

In the past decades several subsurface stratigraphic works were aimed to define Late Quaternary continental shelf prograding deltaic deposits, commonly developed in Mediterranean sea coastal regions. These deposits cross the shelf as the result of the stacking of lowstand system tracts of the 4th order depositional sequences with seaward shifting of coastal facies bounded by polygenetic unconformities. The distribution, lateral extent and thickness of these prograding deposits and preservation potential are also controlled to a large degree by accommodation space below the lowstand shoreline, sediment input, hydrodynamic regime of the receiving marine basin and tectonism (Swift et al. 1991; Trincardi and Field 1991; Chiocci et al. 1997; among others).

According to Suter and Berryhill (1985) and Porebski and Steel (2003) deltaic prograding clinoforms on the middle shelf tend to be at lower angle than that occurring near the shelf edge. These differences are linked to increased accommodation when the deltaic shoreline reaches deeper water. On the contrary, the sea-level rise transforms the deltaic shorelines into estuaries controlled by marine (waves and tides) and fluvial processes.

Published online: 18 April 2014

The wave-dominated estuaries construct small, elongated bayhead deltas, located at the landward end of flooded valleys (Dalrymple et al. 1992; Nichol et al. 1996).

The mineralogy of siliciclastic deposits, as well as the sedimentation rates off the river mouth, may significantly vary according to the geology and size of the drainage river basin inland (Reading 1996).

Among geological processes which are effective in delivering coarse-grained sediments beyond the nearshore areas to the shelf environment are important the formation of density currents originated by sediment failure from an overcharged delta front and shoreface (Wright 1977; Wright et al. 1988), winter storms and hurricane wave actions, which induce combined downwelling currents (Duke 1985, 1990) and, principally for small size rivers with a large sediment/freshwater ratio, the hyperpycnal flows at river mouths (Mudler and Syvitski 1995).

It is generally accepted that prodelta sediments, due to their relatively high preservation potential associated with good vertical and lateral continuity of stratigraphic successions deposited below the storm wave base level, are of particular interest in the study of both modern and ancient marine deltaic environments (Einsele 2000 and references therein). Prodelta sediments are typically represented by fine-grained deposits delivered by a river, reflecting episodes of minor/major river supply.

The prodelta sediments are also commonly dominated by products of mass movements derived from the delta front (Coleman 1988), high sedimentation rates, seabed flow liquefaction triggered by earthquakes (Christian et al. 1997), sediment deformation and slope failure phenomena (e.g. Correggiari et al. 2001; Lykousis et al. 2003), strong action of bottom currents (e.g. Trincardi and Normark 1988), combined action of bottom currents and sediment deformation (e.g. Cattaneo et al. 2004) or hyperpycnal flows bottom currents and regional sea water circulation (e.g. Urgeles et al. 2007) and recently processes in the bottom boundary layers (Urgeles et al. 2011).

During the past few decades, exploration by means of high-resolution swath bathymetry and subbottom profiling of the Campania margin (including several delta systems) coupled with sedimentologic, petrophysic, paleomagnetic and tephrostratigraphic analysis of marine deposits (Buccheri et al. 2002; Iorio et al. 2004a, 2009, 2014; Sacchi et al. 2005; Budillon et al. 2005, 2012; Lirer et al. 2013) has provided valuable insights into its environmental and climatic evolution. In this study an approach, based on high-resolution multiproxy analysis, was applied to define sedimentary and deformation processes of highstand outer shelf deposits of the Campania margin interested by recent Volturno prodelta deposition.

2 Regional geological setting

The investigated area is located in the northern Campania continental margin, between the Volturno mouth and the Cuma town (Fig. 1). The northern Campania plain and its margin form a part of a large extensional Plio-Pleistocene basin associated with normal and strike-slip faults linked to the evolution of the eastern Tyrrhenian Sea margin (Bartole et al. 1984; Malinverno and Ryan 1986; Casciello et al. 2006). Since mid-late Pleistocene, extensional tectonics were accompanied by the onset of an intense volcanic activity which took place across the continental margin from several volcanic districts (Scandone et al. 1991; De Vivo et al. 2001; Milia et al. 2003) of which the Phlegraean Fields, with the last major eruption at 15 ky BP (Neapolitan Yellow Tuff, NYT; Deino et al. 2004) and relative quiescence of Phlegraean Fields caldera from 3.8 ky BP (Di Vito et al. 1999; De Vita et al. 1999; Orsi et al. 2004 and reference therein), is the closest to the study area (Fig. 1).

During the early Pleistocene the Campania continental margin was involved by a strong tectonic subsidence. As a consequence, the northern Campania plain, including the Volturno river segment was submerged by the sea during the middle-late Pleistocene (Mariani and Prato 1988; Florio et al. 1999; Bruno et al. 2000; Aiello et al. 2011). Rapid flooding of lower Volturno Plain was promoted by the latest Pleistocene–early Holocene (ca. 15 ky–6 ky BP) sea-level rise, leading to a generalized widening of the shelf. Since ca. 6.5 ky cal BP, the highstand relative sea level conditions marked the onset of the present Volturno delta and the progradation (3–6 km) of the adjacent coastal plain (Barra et al. 1996; Bellotti 2000; Romano et al. 2004; Amorosi et al. 2012). In the studied area the continental shelf, gently sloping seaward, is as wide as 16 km in front of the Volturno river and narrows southward reaching its minimum width in correspondence to Cuma ($\sim$10 km); the shelf break is located between 120 m and 125 m depth. The upper Pleistocene-Holocene stratigraphic architecture of the continental shelf in the studied area is characterized by a 4th order depositional sequence supplied by deltaic systems genetically linked to the Volturno river and evidenced by related sedimentary architecture, showing an internal organization with minor downlap surfaces and erosional truncations that separate different phases of progradation (Marani et al. 1986; Aiello et al. 2000, 2011). The last progradation started at about 100 ky BP and ended at about 18 ky BP during the Last Glacial Maximum (Chappell and Shackleton 1986). An abrupt erosional surface separates the forced regression and lowstand deposits from the overlying sediments that were formed from about 18 to 5 ky BP during the last sea level rise and from about 5 ky BP to present during the actual sea level highstand (Hunt and Tucker

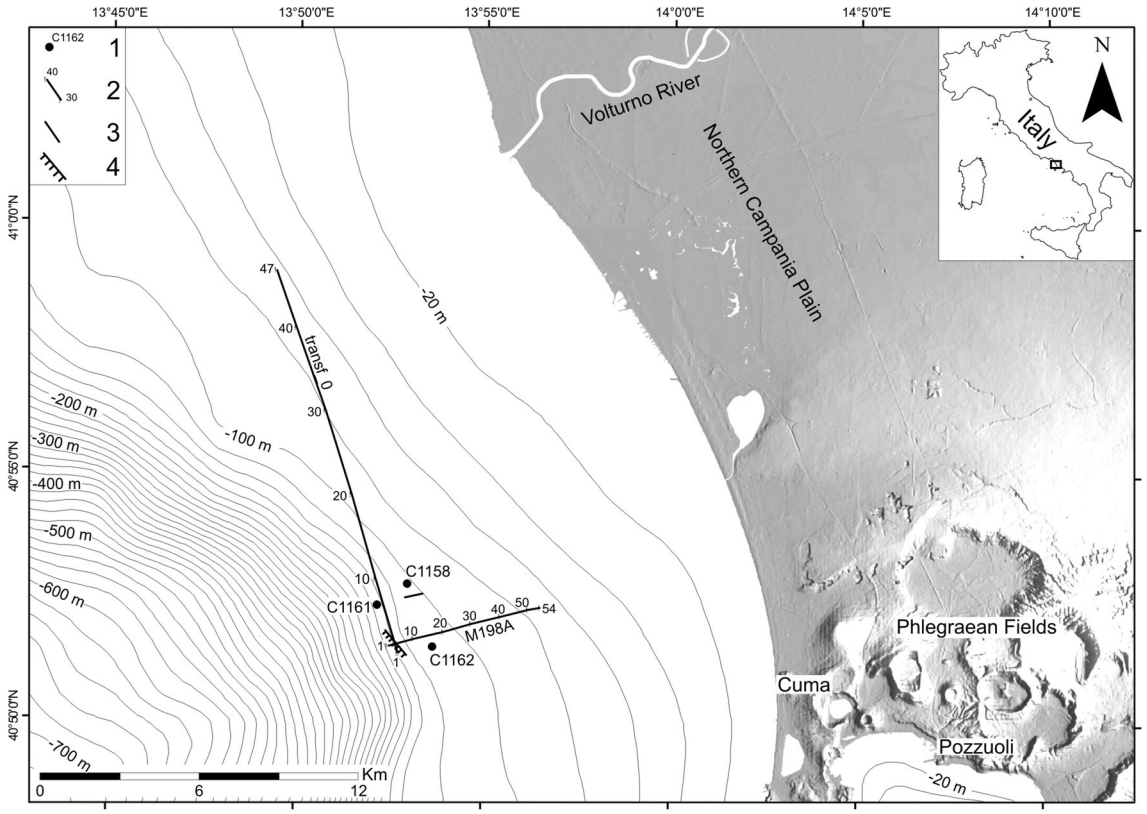

Fig. 1 The Phlegraean Fields offshore and the study area with the dataset of the present research. (1) Cores; (2) Chirp profiles; (3) Fig. 2 inset C; (4) shelf break in the studied area

1992; Amore et al. 1996; Coppa et al. 1996; Buccheri et al. 2002; Ciampo 2003; D'Argenio et al. 2004).The upper Holocene depositional unit consists of a wedge decreasing in thickness towards the shelf edge. Offshore to the present-day prominent Volturno delta, which developed on the maximum flooding surface of the last glacial depositional sequence (Bellotti 2000; Amorosi et al. 2012), it is possible to identify a pronounced seaward convexity of the isobaths that could be related to the ancient river mouth (Pennetta et al. 1998) shifted seaward during the last glacial cycle when the sea level reached the maximum depth of 120 m (De Pippo et al. 2004). The slope is characterized by a uniform profile and is incised by several submarine gullies (Chiocci and Casalbore 2011). The Volturno River is the longest river (175 km) in southern Italy and is characterized by a catchment basin of 5,634 kmq and a maximum river discharge of 102 m^3/s (Chiocci and Casalbore 2011). The Volturno River delta is characterized by a dissipative-type shoreline (Wright et al. 1979; Orton and Reading 1993) with two orders of subaqueous sand bars (Cocco et al. 1988) and a reduced river sediment supply because of an artificial dam close to the river mouth. So far the littoral, which has resulted in a significant retreat of the shoreline since 1909 (Cocco and De Pippo 1988), shows a dynamics where medium-fine sands are moved by beach drift as well as by longshore currents parallel to the coastline (De Pippo et al. 2004). In Bellotti (2000) a wave-dominated delta model was proposed for the present Volturno river. The delta body shows a composite geometry with a tabular and lenticular inner and outer part of few and of about seventy metres of thickness, respectively. The delta front shows a gently sloping flat bottom between 0 and −20 m and littoral bars are present only close to the beach. The prodelta area instead shows a slightly steep bottom as far as 0.46° with convex profile and represents an area, below the storm wave base level, of fine-grained passive deposits, delivered by fluvial water plume and reflecting episodes of minor/major river supply. In relation with this sedimentary model, past sediment deposition influx in prodelta and slope area by hyperpycnal flows were proposed by Chiocci and Casalbore (2011), linked to the sudden and large supply of loose tephras in the Volturno river catchment basin.

3 Materials and methods

3.1 Seismic data acquisition

Two Chirp profiles (penetration of 25–50 m below the sea bottom using an average velocity of 1,550 m/s for time to

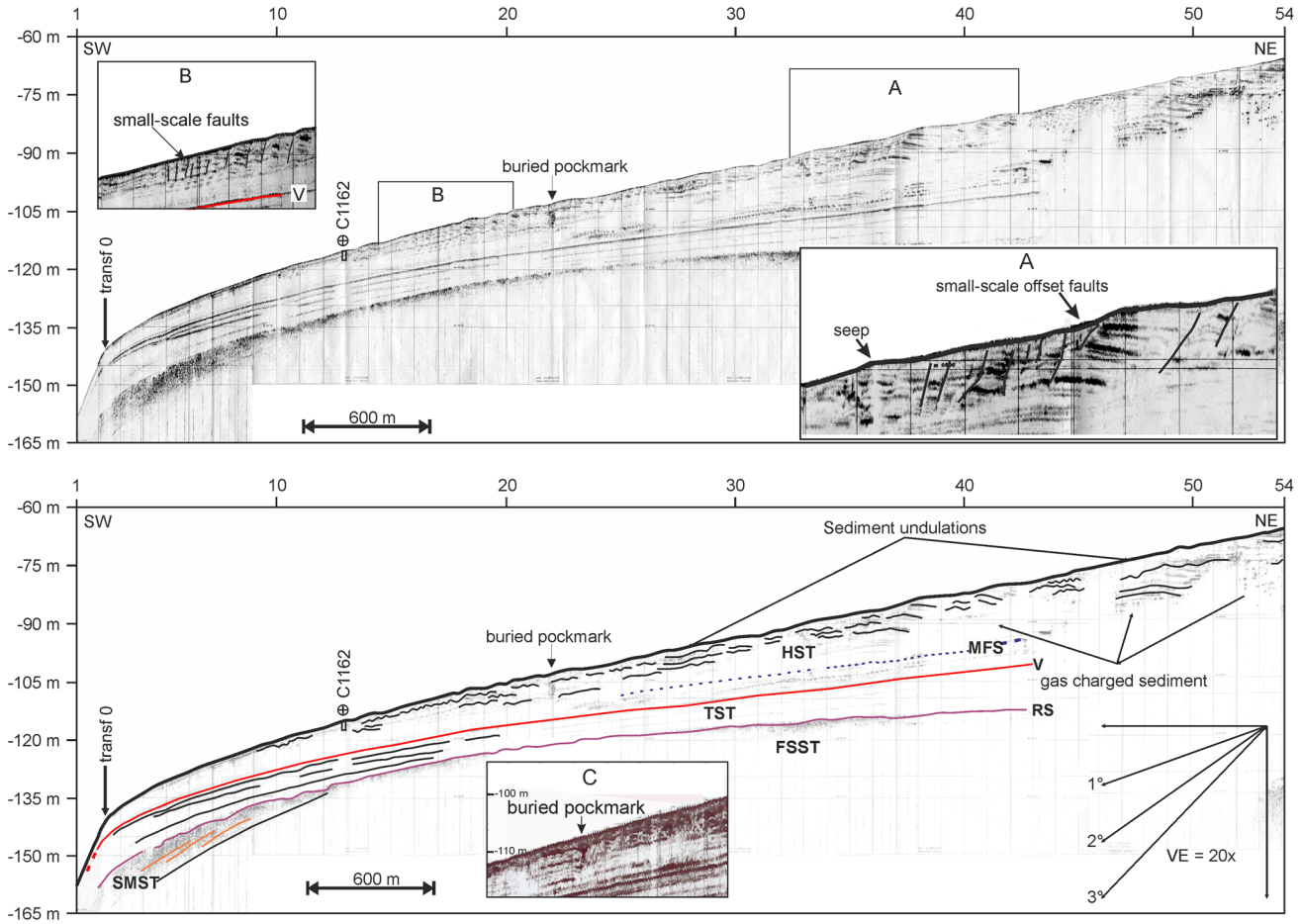

Fig. 2 M198A Chirp profile (location in Fig. 1) and its line drawing. FSST and SMST units: prograding deposits emplaced during Late Pleistocene. *RS* ravinement surface, *TST* transgressive systems tracts, *MFS* maximum flooding surface, *HST* highstand systems tracts. Submarine sediment undulations, diffuse shallow gas pockets and Transf_0 chirp profile and core C1162 (not to scale) projections are shown (modified by Petruccione et al. 2011). A, B and C insets show small-scale offset faults, seeps and pockmarks

depth conversion), one NW–SE and the other one NE–SW oriented are considered to provide a stratigraphic framework for insertion of the analysed gravity cores. Positioning was established through the Starfix Differential GPS (Figs. 1, 2, 3).

3.2 Gravity core sampling

A gravity corer 6 m long with liners 9 cm in diameter was used to collect cores. Three cores are analysed in this study (Table 1). Cores C1158 and C1162 (Petruccione et al. 2011) were recovered on the outer shelf while C1161 (Fig. 1) was recovered on the right side of an upper slope gully. The cores penetrated some 6 m into upper Holocene deposits and core recovery was about 50 % in cores C1158 and C1161 and 65 % in core C1162, while compaction was estimated to be roughly 15 % in each core. The cores were split in two halves, photographed, described for lithostratigraphic analysis and used for continuous high-resolution petrophysical and sedimentological analysis.

The lithostratigraphic analysis of sediment cores was based on the macroscopic characters of the sediment according to the standard methodology (e.g. Tucker 1988). Representative stratigraphic logs listing these characters and the presence of gradual, sharp and erosional contacts, were produced (Fig. 4).

3.3 Grain size analysis

The analysis of grain size in samples collected at 5 cm intervals along the cores was performed according to standard methodology (Folk 1965) and provided the data for textural characterization of the sediment cores. Particles coarser than 63 μm were analysed by sieving. The <63 μm fraction was analysed by sedimentation method. First, sodium oxalate and distilled water were added to the

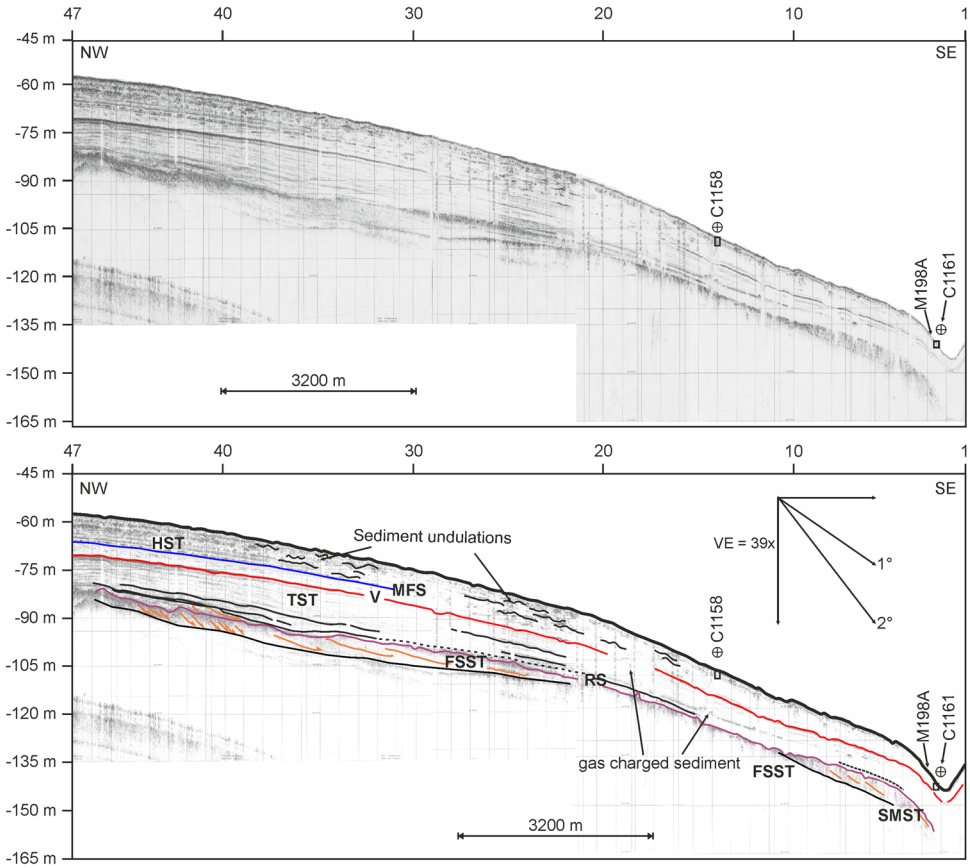

Fig. 3 Transf_0 Chirp profile (location in Fig. 1) and its line drawing. Seismic units and surface labels as in Fig. 2 legend. The upper HST unit shows submarine sediment undulations and diffuse shallow gas pockets. Gravity cores C1158 and C1161 (not to scale) and M198A chirp profile projections are shown

Table 1 Location and details for gravity cores discussed in this study

Gravity core	Location	Depth below see level (m)	Core recovery (m)	Distance from the coast (km)
C1158	40°52′45.24″N 13°53’0.22″E	−108	2.54	12.5
C1168	40°52′13.80″N 13°51′41.80’’E	−144	2.62	14.5
C1162	40°51′31.80″N 13°53′42.00″E	−115	3.54	12.4

compound, then it was shaken and the suspension percentage was sampled using a 20-ml pipette, following the drawing times of Belloni (1969). The statistical parameters of Folk and Ward (1957) were calculated from cumulative curves of analysed sample, and the percentages of gravel, sand, silt and clay fractions were calculated for each sample (Fig. 5).

The sediment was classified using the triangular diagram of Shepard (1954) modified according to Folk (1965) and, to obtain further information, the method of Passega (1957, 1964, 1977) was used. This method, based on textural analysis of sediments from present-day continental, transitional and marine environments, allows to identify, for each environment, sediment patterns associated with different transport and deposition mechanisms. The integration among lithostratigraphic and grain size analyses and data obtained from Passega diagram were useful for the final definition of the depositional environments.

The percentages of all the sampled fractions and the calculated statistical parameters were plotted versus stratigraphic depths in the studied cores (Fig. 5).

3.4 Petrophysics measurements

The physical properties of the cores, Volume Magnetic Susceptibility (VMS), Gamma Ray Density (GRD) and Diffuse Reflectance Spectra (DRS), were measured at 2 cm intervals using a fully automated GEOTEK Multi-Sensor Core Logger (MSCL) at the CNR-IAMC petrophysical laboratory (Fig. 6). The VMS, GRD and DRS measurements were obtained through a Bartington MS2E Point sensor, a Gamma Ray Attenuation Porosity Evaluator (GRAPE) system and a Minolta Spectrophotometer CM-2002, which records the percentage of reflected energy from the surface of each sample (sample’s spectrum) relative to a white (BaSO4 standard) ceramic tile cap, in 10 nm wavelength steps, over the visible domain (400–700 nm).

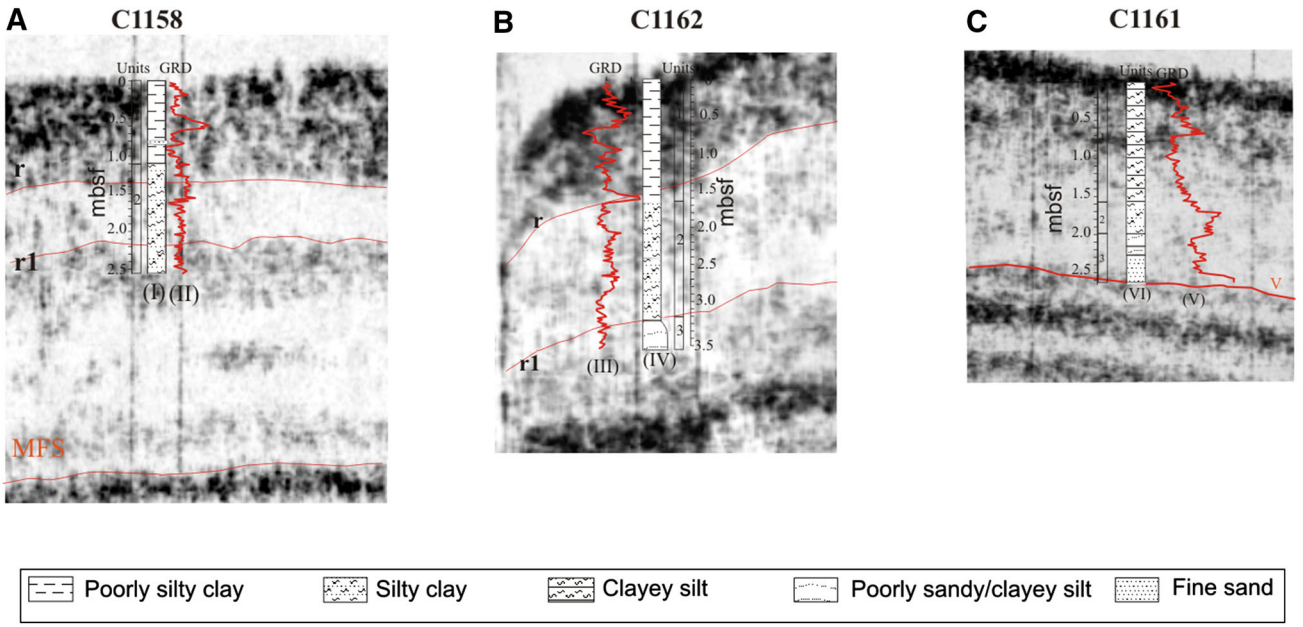

Fig. 4 Sedimentological-petrophysical logs and projections on seismic profiles for cores C1158, C1162 (Petruccione et al. 2011) and C1161 (This study). **a–c** Raw GRD data (*II*, *III* and *V*) and sedimentological logs (*I*, *IV* and *VI*) of C1158, C1162 and C1161 projected against the related seismic profiles and showing the correlated changes of sedimentation (Units 1–3), seismic horizons (r, r1 and V in A, B and C respectively) and density values (see text for details). Sedimentological legend as in figure

Analyses were carried out using a D65 illuminant, which corresponds to average daylight, with a colour temperature of 6,504 K and an 8-mm aperture.

The measured Diffuse Reflectance Spectra (DRS) values were also used to collect information on sediment colour, since the measured reflectance of a specific spectral energy distribution, under standardized conditions, was converted to the L*a*b* colour indices. The L*a*b* colour scheme, which is based on human perception, consists of a brightness component L* and a* (red to green) and b* (yellow to blue) representing the chromaticity parameters (CIE 1978 and Minolta CM-2002 handbook). The petrophysical measurements were undertaken about 0.5 h after the cores were split, (Debret et al. 2006) to minimize any drying or oxidation effects on the magnetic, geochemical and mineralogical properties. Technical characteristics of the Minolta spectrophotometer (set to exclude the specular component) and the methods for acquiring the reflectance spectra are those presented by Balsam et al. (1997).

Afterwards, the petrophysical data, averaged out with a 5-cm window, were visually and mathematically compared to detect similar trend of curves and correlate to the lithological properties according to their physical properties.

The numerical method used to compare and correlate petrophysical properties was provided by the interactive program SPLICER on Unix platform. This software was developed at the Lamont Doherty Earth Observatory (Hagelberg et al. 1992) to enable petrophysical data from several cores to be viewed simultaneously. The program then establishes correlations between the properties within each core and then overlays the data from one core with those from the others. The two (or more) sets of data are statistically compared after wiggle matching until an optimum correlation is obtained on the basis of cross-correlation functions. A common synthesis is then derived that gives the depth-shifts needed to convert from the metric scale below sea floor (mbsf) to a common metre composite depth (mcd) (Fig. 7).

4 Results

4.1 Seismic-stratigraphic framework

Seismic-stratigraphic interpretation was carried out on the two high-resolution Chirp profiles (Fig. 1), acquired close to the studied cores, allowing definition of the stratigraphic framework characterizing the area under interest. Stratigraphic surfaces bounding seismic units have been recognized. The latter, constituted by relatively conformable successions of reflectors, were interpreted basing on their internal and external geometries and considering their seismic facies (Vail et al. 1977, 1991; Van Wagoner et al. 1988; Posamentier et al. 1992; Catuneanu et al. 2009; Zecchin and Catuneanu 2013).

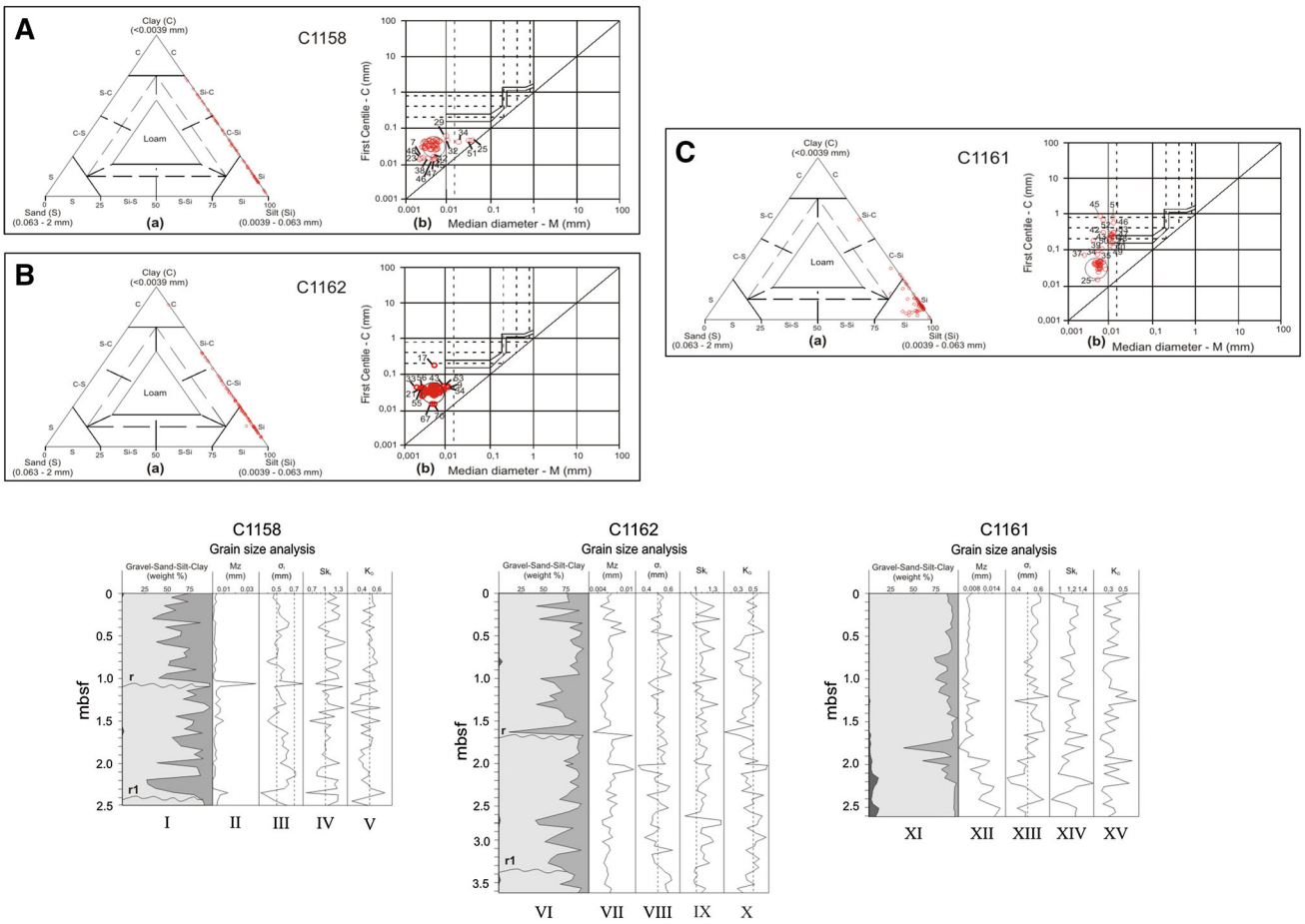

Fig. 5 Grain size analysis. **A–C** Cores C1158, C1162 (Petruccione et al. 2011) and C1161 (This study). (*a*) Classification diagram modified after Shepard (1954) and (*b*) C-M (*C* the one percentile, *M* the median diameter) diagram of Passega (1964). Legend for triangular diagram: *S* sand, *C–S* clayey sand, *S–C* sandy clay, *C* clay, *Si–C* silty clay, *C–Si* clayey silt, *Si* silt, *S–Si* sandy silt, *Si–S* silty sand. *I*, *VI* and *XI:* The variation versus depth of gravel, sand, silt and clay fractions concentration. *II* to *V*, *VII* to *X* and *XII* to *XV*: The variation versus depth of the Folk and Ward (1957) statistical parameters. Legend for columns II to V, VII to X and XII to XV: *Mz* Graphic mean, *σi* inclusive graphic standard deviation, *Ski* inclusive graphic Skewness, *Kg* graphic kurtosis

The oldest unit (Falling Stage System Tract, FSST) is constituted by reflectors with moderate amplitude and continuity, which are in offlap towards SW with about 1° of slope and bounded on top by an erosional surface. The FSST is characterized by downlaping clinoform reflectors (Fig. 3) which seaward incurred a wedge-shaped unit (Shelf Margin System Tract, SMST). The erosional surface (Ravinement Surface, RS), that represents the upper boundary of both FSST and SMST units, is a well-marked horizon deepening towards sea (Figs. 2, 3). The transgressive unit (Transgressive System Tract, TST) lies in onlap on the RS surface and is characterized by parallel and continuous seismic reflectors with a low amplitude (Figs. 2, 3). Inside this unit, a conformable reflector (V) characterized by high continuity and amplitude is continuously detected on the shelf and upper slope, recognizable on both profiles (Figs. 2, 3). The TST unit boundary has been identified on the Transf_0 profile (Fig. 3) and is represented by the Maximum Flooding Surface (MFS) reflector.

Above the MSF surface lies the uppermost unit (Highstand System Tract, HST) which is characterized by discontinuous seismic reflectors with moderate to high amplitude, occasionally affected by shallow gas pockets, which hide the acoustic signal. The HST unit thickness decreases towards the shelf break (Figs. 2, 3). The HST unit reflections are interested in our profiles by several undulations in the upper most part of the unit, from about −70 m to about −120 m where the shelf gradient deepens from about 0.2° to 0.5°. Within the undulated reflectors individual packets can be distinguished, separated by small scale, differently oriented, extensional offset faults (Fig. 2 inset A and B) which slightly downthrow internal reflectors, extending to a mean depth of 6 m below seafloor

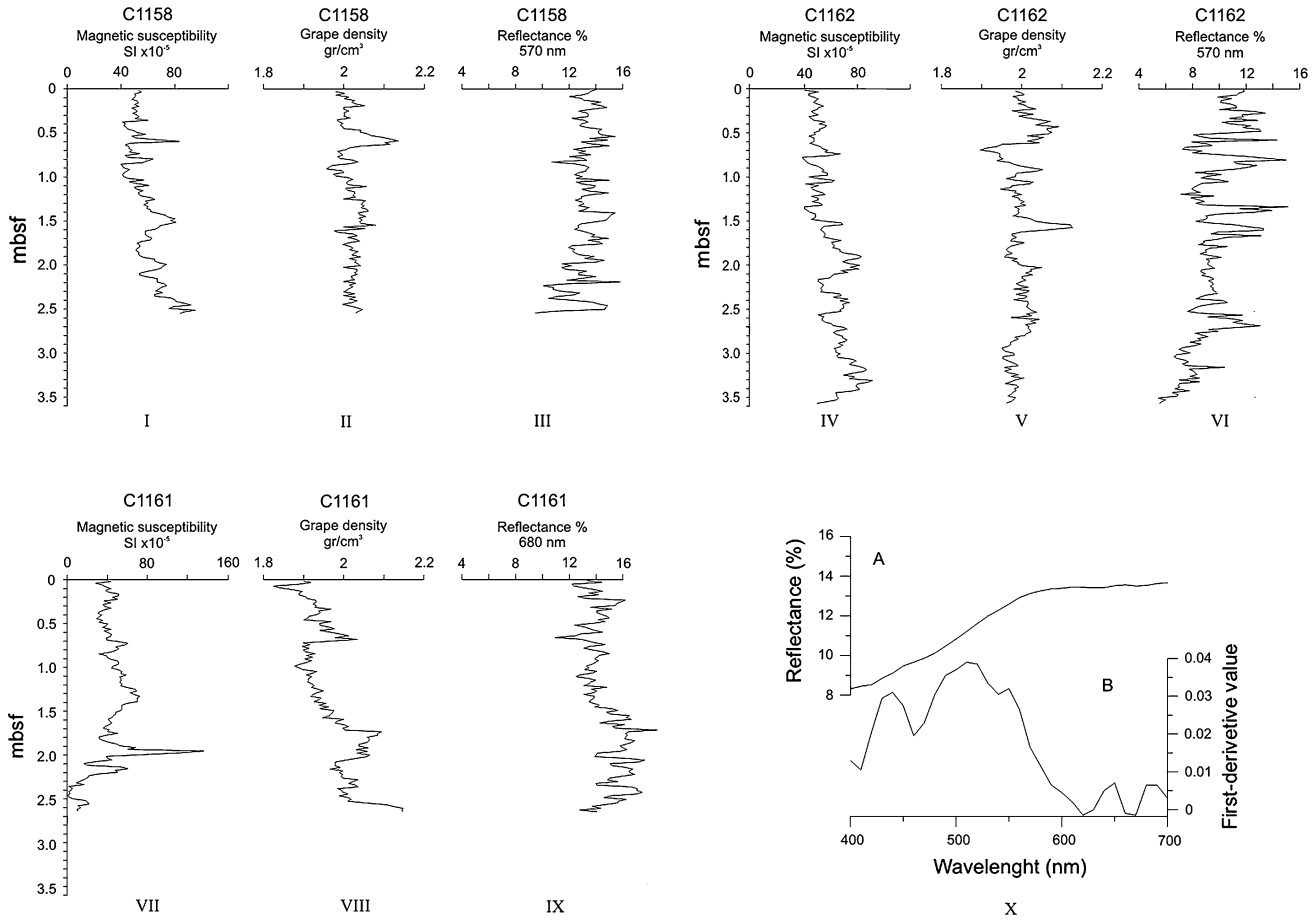

Fig. 6 Petrophysical data logs and first derivative of the Diffuse Reflectance Spectra. *I–IX* High-resolution petrophysical properties of cores C1158, C1162 and C1161: VMS raw data (*I*, *IV* and *VII*); GRD raw data (*II*, *V* and *VIII*) and DRS 570 and 680 nm raw data (*III*, *VI* and *IX*) plotted against meter below sea floor (mbsf). *X* Core C1158 average Diffuse Reflectance Spectra of all samples within sections where high susceptibility values were found (*A*). First derivative of the Diffuse Reflectance Spectra in *A* (*B*). The distinct peaks at 555 and 435 nm indicate that in such intervals a mixture of hematite and of other iron oxides is present (Balsam and Deaton 1991)

above the same physical plane. The individual packets show internal slightly counter-slope dipping, are asymmetric having a steeper down slope side and are equally distributed with a constant amplitude (about 50 m) in the downslope direction (Fig. 2 inset A and B).

Towards the shelf break an abrupt change in the sea floor gradient is recorded (Fig. 3) and actual fluid escape features (pockmarks, seeps) define the undulated deposits. Several buried pockmarks, sealed by about 2 m of sediment from seafloor, testify that this process was active also in the recent past (Fig. 2, inset C).

4.2 Sedimentologic analysis

Sedimentological observations of the three gravity cores, recovered within the upper Holocene HST unit (Figs. 1, 2, 3), were performed at a centimetre-scale and the logs are shown in Fig. 4a-I, b-IV and c-VI. Grain size analysis indicates that the sediment is mainly silt and clay, with the sand and gravel fraction being present in very low percentages; the triangular diagram (Fig. 5, A-a; B-a and C-a) classifies the analysed samples as silt, clayey silt and silty clay. Nevertheless, some differences between the three cores can be recognized.

Both cores C1158 and C1162 are mainly composed of olive fine to very fine silt; the median diameter falls between 3 μm and 8 μm and the sand and gravel fraction is absent or <1 %; the sediment is moderately to poorly sorted, reach in water content and shows mainly coarse skewed and leptokurtic grain size distributions (Fig. 5, II–V and VII–X).

Although the C-M pattern of Passega (1957, 1964, 1977) for these deposits is typical of an environment with quiet waters (Fig. 5, A-b and B-b), where very fine sediments settle without being sorted, the alignments of shell fragments recognized within the coarser levels testify the

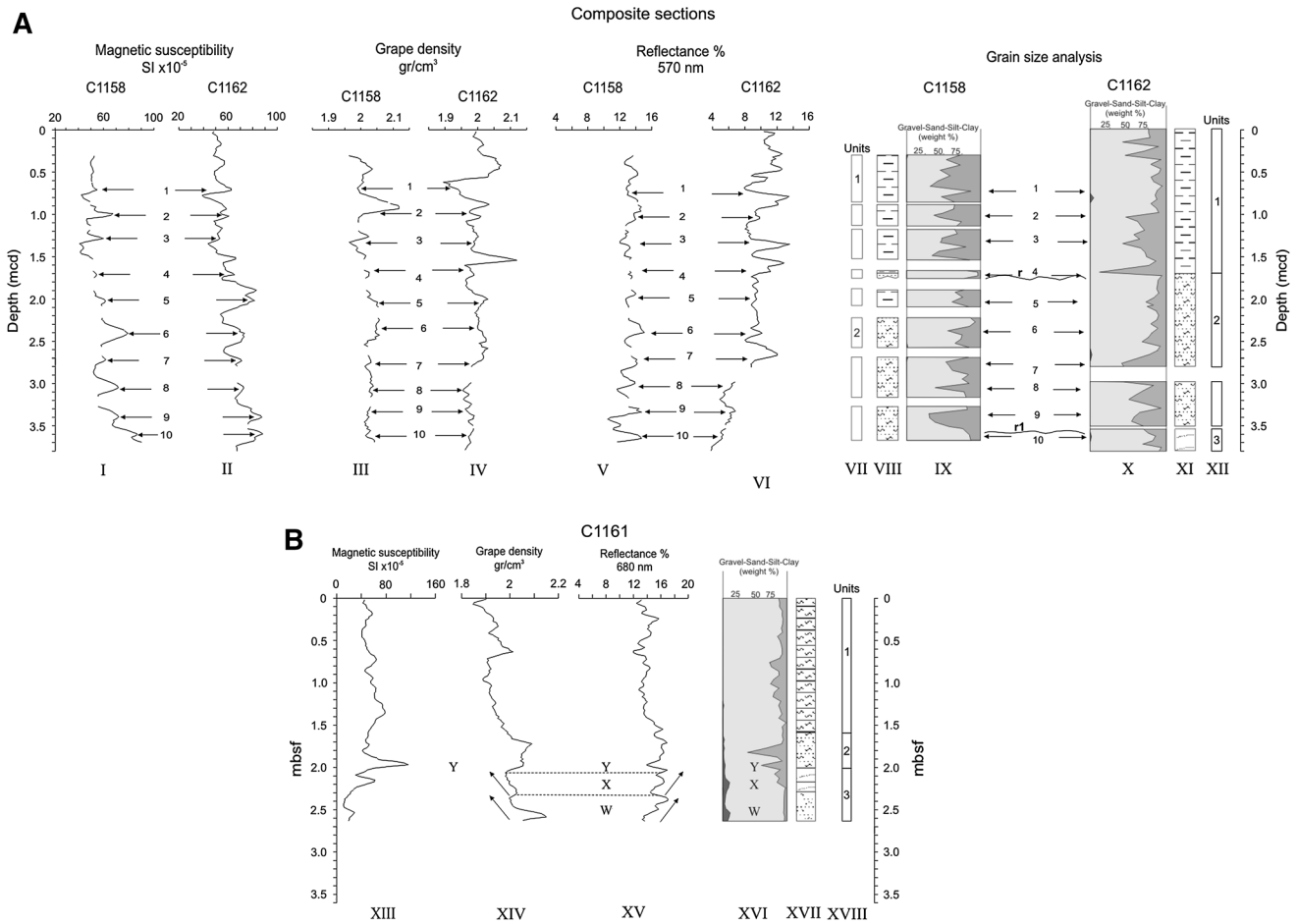

Fig. 7 Correlation and comparison of petrophysical–sedimentological data sets. **a** Composite sections of high-resolution smoothed petrophysical properties of core C1158 and C1162: VMS data (*I*, *II*); GRD data (*III*, *IV*) and DRS 570 nm data (*V*, *VI*). The numbers 1–10 indicate synchronous events of petrophysical (*I–VI*) and grain size (*IX*, *X*) variations, occurring in the measured cores. (See text for details). **b** High-resolution smoothed petrophysical properties of core C1161: VMS data (*XIII*); GRD data (*XIV*) and DRS 680 nm data (*XV*). Labels *X* and *W* in columns *XVI* (unit 3) indicate graded coarse/silty sediments, fining upward to muddy levels. In columns *XIV* and *XV arrows* indicate density and reflectance systematic variations, occurring in the graded *X* and *W* intervals (see text for details). Label *Y*, in columns *XIII*, *XV* and *XVI* indicates a volcaniclastic level

occurrence of higher energy events. The sediment contains volcanic and bioclastic components. The volcanic component is mainly black ash and/or millimetre-size grey pumice clasts. The bioclastic component is represented mainly by Mollusk shell fragments; rarely, parts of Echinoids can be recognized. Interspersed within this sediment are several levels of finer (clayey silt or silty clay) and coarser (medium silt) poorly sorted sediment, showing platykurtic curves.

These data suggest a continuous and undisturbed distal sedimentation typical of an aggrading/prograding continental shelf, also supplied by the contribution of volcanic/volcaniclastic deposits and storm events (coarse-grained levels). The macroscopic sedimentological observations together with grain size analysis allowed us to subdivide both core logs into three sedimentological units (r1 and r limits; Figs. 4a and b, 5 I and VI).

In core C1161 two different parts can be distinguished (Figs. 4c, 5XI). The first part (0–1.57 m; Unit 1) is constituted by silt and clay sediments, similar to that recognized in the C1158 and C1162 cores, even though the clay fraction is represented by lower percentages and the sediment is better sorted.

In the second part of the core (1.57–2.62 m; Units 2 and 3), three fining upward successions can be recognized. They are constituted by olive grey medium silt at the bottom grading to olive fine silt at the top; median diameter falls between 6 μm and 13 μm, and the sand fraction reaches 10 % in concentration. As in the other two cores, the sandy component is constituted mainly of volcanic ash and bioclastic elements, while the gravel fraction is made of millimetre-size pumice clasts; the sediment is moderately to poorly sorted and shows mainly coarse skewed and leptokurtic grain size distributions. In this lower part, the

CM pattern of Passega (1957, 1964, 1977) falls beyond the quiet waters field and approaches the tractive currents field (Fig. 5C), in which fine particles settle with intermediate and coarse size particles. These data, together with the occurrence of alignments of pumice clasts, of shell fragments (mainly Mollusks and Echinoids) and fish teeth at several heights in this level, indicate a higher energy depositional environment, which is in agreement with the location of the core on the right side of an upper slope gully.

4.3 Petrophysic analysis

Physical properties of soft sediments are generally considered good indicators for sediment composition, formation and environmental conditions. MSCL petrophysical analysis are commonly used for high-resolution correlations over wide oceanic and volcanic district marine areas, providing information on sediment provenance, regional stratigraphy, palaeoclimate and tephrostratigraphy (Robinson et al. 1995; Moros et al. 1997; Ortiz and Rack 1999; Helmke et al. 2002; Giosan et al. 2002; Iorio et al. 2004a, 2009, 2014; Miao et al. 2007; Vallefuoco et al. 2012; Lirer et al. 2013). Moreover, VIS reflectance spectra and pre-treatments (including calculation of the first or second derivative or various functions such as logarithm, polynomials, etc.), applied to the raw spectra, have been used in sediment to identify iron oxide and oxyhydroxide minerals, clay minerals, calcite, sediment organic content and grain size variations in alternating high/low depositional energy environments (Barranco et al. 1989; Deaton and Balsam 1991; Herbert et al. 1992; Balsam and Deaton 1991, 1996; Mix et al. 1995; Balsam et al. 1999; Ortiz et al. 1999; Wolf-Welling et al. 2001; Balsam and Beeson 2003; Debret et al. 2006; Balsam et al. 2007).

In particular, changes in particle size are known to cause variation in overall sample reflectivity and in absolute band intensities (Gaffey 1985). However, variations in reflectivity resulting from grain-size differences appear to be minimized by the relatively small size range, primarily silt and clay, exhibited by deep marine sediments (Barranco et al. 1989).

So far it was decided to investigate, within cores mainly characterized by silt and clay (C1158 and C1162), the detailed correlation among Magnetic Susceptibility, Grape Density and Diffuse Reflectance Spectra variations, the latter at a wavelength range known to be sensitive to iron content. In fact these cores were collected in a quiet depositional environment (as shown by sedimentological analysis), which was enriched by several iron oxide minerals probably due to feeding from volcanic district area, as evidenced by the positive magnetic susceptibility values. First-derivative analysis of the sediment reflectance spectrum was used to choose the iron-sensitive wavelength range, a processing method previously used to identify iron oxide minerals in marine sediments, especially hematite and goethite (Barranco et al. 1989; Balsam and Deaton 1991; Deaton and Balsam 1991). In fact, hematite has a single prominent first derivative peak centred at either 565 or 575 nm, whereas goethite has two first derivative peaks: a primary peak at 535 nm and a secondary peak at 435 nm. In practice, the 435-nm peak is a better indicator of goethite because the 535-nm peak is commonly obscured by hematite (Balsam and Damuth 2000; Balsam and Wolhart 1993). So far it was found that the first-derivative curve of the reflectance data for cores C1158 and C1162 (example in Fig. 6X) was consistent with a mixture of iron oxides (goethite, hydrated oxides and hematite) (Barranco et al. 1989; Balsam and Deaton 1991) and the DRS at 570 nm wavelength, which is sensitive to hematite contents (Deaton and Balsam 1991), was used to check a positive correlation with higher susceptibility values in the lower energy depositional environment.

Furthermore, for core C1161 which was instead collected from a depositional environment characterized by high energy (as shown by the seismostratigraphic and sedimentological analysis), and recorded more grain size variations than cores C1158 and C1162, it was decided to mainly check the relationship between variations of Grape Density and DRS at 680 nm wavelength value and this wavelength range was also chosen after first derivative analysis of the Diffuse Reflectance Spectra of the core, as it was known to be sensitive to grain size variations (Wolf-Welling et al. 2001 and references therein).

Mean values of measured parameters were calculated for all cores and found to be very similar to each other; the values ranged between 58.6, 61.8 and 50.6 SI $\times$ 10^{-5} for VMS data, between 2.01, 1.99 and 1.97 gr/cm^3 for GRD data, between 12.9 and 9.6 % for DRS 570 nm data and 14.4 % for DRS 680 nm, respectively, in cores C1158, C1162 and C1161.

As shown by the logs (Fig. 6I–IX), the petrophysical data, from top to bottom, are characterized by a wavering pattern around mean values with several distinct peaks, mostly of high amplitude, for cores C1158 and C1162.

However, core C1161 GRD and DRS 680 nm data show, with respect to their mean, lower and higher wavering pattern values in the first 1.5 m and in the remaining 1.0 m, respectively.

A visual check showed a noticeable correspondence between core C1158 and C1162, but not with core C1161. To compare the petrophysical features between the corresponding cores (C1158 and C1162), the data for each core, smoothed out with a 5-cm window, were processed

statistically comparing the different wiggle matching of each petrophysical data set from one core with that from the other, until an optimum correlation, based on cross-correlation functions, was established (Hagelberg et al. 1992).

It was found that in the depth intervals ranging from 0.28 to 2.54 and 0.52 to 3.41 mbsf for C1158 and C1162, respectively, the data show a very good correlation among the VMS values and fairly good correlation for the GRD and DRS570 values, despite the fact that the chromaticity values of core C1158 are slightly higher with respect to C1162. In Fig. 7a the correlated C1158 and C1162 petrophysical parameters have been plotted against the common scale depth (meter composite depths: mcd) derived by the SPLICER software output (Fig. 7a, I–VI). As it is possible to notice from correlation the upper part of core C1158 seems about 30 cm shorter than core C1162, probably due to the loss of sediment that occurred during coring (Fig. 7a).

Afterwards, we analysed the data in more detail and attempted to identify single prominent and highly informative peaks and troughs in the mathematically correlated portion of datasets. This process is aimed at obtaining a high-resolution (centimetres scale) correlation between the two cores. From this procedure, we were able to define ten homologous points at the same interval depths (±5 cm) on both cores in all petrophysical logs (Fig. 7a, I–VI).

4.4 Sedimentological–petrophysical correlation

The obtained petrophysical correlation for core C1158 and C1162 were then checked within the remaining grain size logs, and it was found that there is a good correspondence with the relative increase of the clay fraction percentage in the sedimentological records (Fig. 7a, IX and X) at the same stratigraphic composite depths for seven out of ten relatively high (VMS and DRS 570 nm) and low (GRD) correlated peaks (Fig. 7a, I–VI). Keeping in mind that there is a lack of studies on reflectance properties behaviour in shelf margin sediments, it is possible that higher relative concentrations of magnetic minerals in clay contents (VMS higher values) correspond to relative high peak values of the DRS 570 nm records, as a consequence of an enrichment of iron oxides.

Also, there are low value peaks for GRD properties, considering the high porosity and the high water content of the clay fraction (Weber et al. 1997). Finally, around sedimentological boundary units r and r1, peaks 4 and 10 correspond to a relative increase of the silt fraction percentage, in line with the marked lithological changes (Figs. 4a, b, 7a, IX and X). So far, coherent correlation of sedimentological and petrophysical parameters from the south-western and north-eastern sectors of the studied area have shown a high-resolution pattern that is comparable within the first 2.5 m of sediment, and we conclude that the correlated upper part of seismographic unit Hu, which was sampled from cores C1158 and C1162, is constituted by the same sedimentological layers (Sedimentologic Unit 1 and 2 in Fig. 4a, b).

Passing to the higher energy sector of the upper slope, sampled from core C1161, the principal changes of VMS, GRD and DRS 680 nm data seem related to the sedimentological macroscopic characters of Units 1, 2 and 3 (Figs. 4c, 7b), except for the VMS and DRS 680 nm high and low peak values (Y in Fig. 7b, XIII–XVI) which are related to an ash layer, which corresponds to the V reflector detected by the seismic analysis (Fig. 3). Moreover, the GRD pattern, in agreement with Weber et al. (1997), shows a strictly linked clay/silt/mud concentration variation (Fig. 7b, XIV and XVI). However, it is also interesting to notice that two of the three graded fining-upward coarse/silty/muddy sediments within unit 3 (Fig. 7b, labels W and X in column XVI), interpreted as deposited in an higher energy depositional environment (gully right side and reworked sedimentation as defined from sedimentological analysis, localization in Fig. 3), show systematic relative density and reflectance variations (Fig. 7b, XIV and XV arrows).

5 Discussion

5.1 Stratigraphic architecture of the Northern Phlegraean offshore

The seismo-stratigraphic interpretations, developed on the base of the Tyrrhenian sea continental shelf knowledge (Marani et al. 1986; Trincardi and Field 1991; Chiocci 1994; Coppa et al. 1996; Aiello et al. 2000, 2011; Buccheri et al. 2002; Aucelli et al. 2012; Budillon et al. 2012 among others), allowed to define the stratigraphic architecture and propose a preliminary chronostatigraphic framework for Late Pleistocene-Holocene sedimentary sequence in the study area.

The occurrence of prograding reflectors in the FSST and SMST units (Figs. 2, 3) suggest that they may represent deposits emplaced during Late Pleistocene sea level fall that lasted up to about 18 ka (Last Glacial Maximum) when the sea reached −120 m with respect to the present sea level.

The RS reflector (Figs. 2, 3) corresponds to a regional unconformity, associated with a time-transgressive landward shift of the fair-weather wave base during the rapid sea-level rise that accompanied the Post Glacial-Holocene deglaciation.

Above the RS reflector, the transgressive unit (TST) emplaced during the sea level rise produces inland shift of

the coastal facies up to the maximum flooding of the sea level (5–6 ky BP). The expression of the maximum flooding sea event is represented by the MFS surface. The downlap geometry of the reflectors above MFS is in some cases obscured by undulations that affect the upper part of HST highstand unit which is interested by small-offset faults extending to a mean depth of 6 m below seafloor, above shear planes developed in the lower part of muddy (probably minor flooding surfaces) or/and gas charged HST sediments which act as a common basal weak layer and detachment surface.

Below the MFS and during transgressive time (18–6 ky), the V reflector is derived by a tephra layer, as confirmed by the petrophysical analysis, probably linked to Phlegraean Field eruptions, which were particularly active at that time (NYT and I and II epochs, Di Vito et al. 1999).

The upper HST unit is composed of prograding deposits emplaced during the Holocene high stand of sea level up to the present day. During this time the onset of the present Volturno delta is established (Barra et al. 1996; Bellotti 2000; Romano et al. 2004; Amorosi et al. 2012).

Finally, we conclude that the SMST, TST and HST units constitute the 4th order incomplete Late Pleistocene—Holocene depositional sequence in which the upper boundary is lacking.

5.2 Sedimentary processes acting in Holocene highstand deposits

5.2.1 Chronostratigraphic constrains

Records of sediment colour spectra can provide superb stratigraphic information and resolve coherent climatic variability at the century scale (Helmke et al. 2002; Iorio et al. 2004b and references therein; Miao et al. 2007; Balsam et al. 2007 and references therein). Since 1996, the reflectance data obtained during the Ocean Drilling Program proved to be extremely helpful as a correlative tool for hole to hole Site splicing, and recently DRS data have been used for correlation of deep-sea sediments coming from different Mediterranean Sea sectors (e.g. Lourens 2004; Budillon et al. 2009). Also, previous studies of North Atlantic deep-sea sediments indicate that the red–green (a*) colour parameter is primarily controlled by the deposition of iron-bearing minerals (e.g. Nagao and Nakashima 1992; Helmke et al. 2002), so considering that the Holocene/Pleistocene sediments in the Campania margin are enriched in volcanic iron-bearing materials and that they are often characterized by cyclic recurrence of sedimentary patterns forced by global climate and sea level variations (Buccheri et al. 2002; Ciampo 2003; Iorio et al. 2009; Sacchi et al. 2009; Vallefuoco et al. 2012), it should not be surprising that fluctuating patterns in the colour reflectance records relative to two close and similar environmental marine areas can be similar.

Therefore, with the aim to assign an age to the recovered sediment undulation facies, a preliminary age model is presented based on the correlation of the chromaticity parameter a* data obtained from core C1158, selected for comparison, despite the lack of the first 30 cm for the remaining regular sedimentation signal and core C836 (Fig. 1, right corner) collected from neighbouring continental shelf areas (Salerno Gulf; Iorio et al. 2004a, 2009). Core C836 was dated by means of high-resolution paleomagnetic and tephrostratigraphic methods (Iorio et al. 2004a; Sagnotti et al. 2005; Lirer et al. 2013) and by ^{14}C and paleomagnetic extrapolated dating established for the Salerno Gulf margin correlated cores C90 and C1201 (Iorio et al. 2009; Sacchi et al. 2009; Vallefuoco et al. 2012; Lirer et al. 2013).

First, a visual comparison was performed for cores C1158 and C836 chromaticity parameter a* data plotted versus depth and time, respectively. Ten time calibration points along the record for C1158 (indicated by stars in Fig. 8a) have been positioned taking into account the lacking of the upper 30 cm of sediments in the core C1158 and using several distinctive directional swings. A preliminary depth–age transformation was obtained by linear interpolation for C1158, assuming that there is a constant sedimentation rate between the sequential pairs of calibrated points. The obtained chromaticity parameter a* C1158 calibrated curve was then compared with the respective chromaticity a* C836 dated curve (Fig. 8b). This comparison shows that the large-scale reflectance fluctuations in core C1158 not only have a similar pattern to those reported in the Salerno Gulf record, but mostly encompass absolute values in the same range (Fig. 8b). However, it is interesting to note that the interval in which the absolute values diverge (in particular with higher C836 a* values) occurs immediately before and after the Vesuvius Plinian Eruption, during which transported tephra greatly affected the southern Campania margin sediments more than the northern margin sediments (Sacchi et al. 2005 and references therein). On the whole, the good visual correlation obtained between the two records allows us to extrapolate the compiled chronology established for core C836 to core C1158, thereby suggesting that the recovered sediments in core C1158 could represent about 2300 years BP (Fig. 8b).

Seismostratigraphic evidence in support of this time estimate is provided by the total thickness of sediment above the MFS boundary, recognized in the seismic profiles (Fig. 4a) which is regionally recognised as occurring at between 7 kyr and 5 kyr (Buccheri et al. 2002; Trincardi et al. 2004; Amorosi et al. 2012). Moreover, the age of the sediment involved in the sediment undulations phenomena

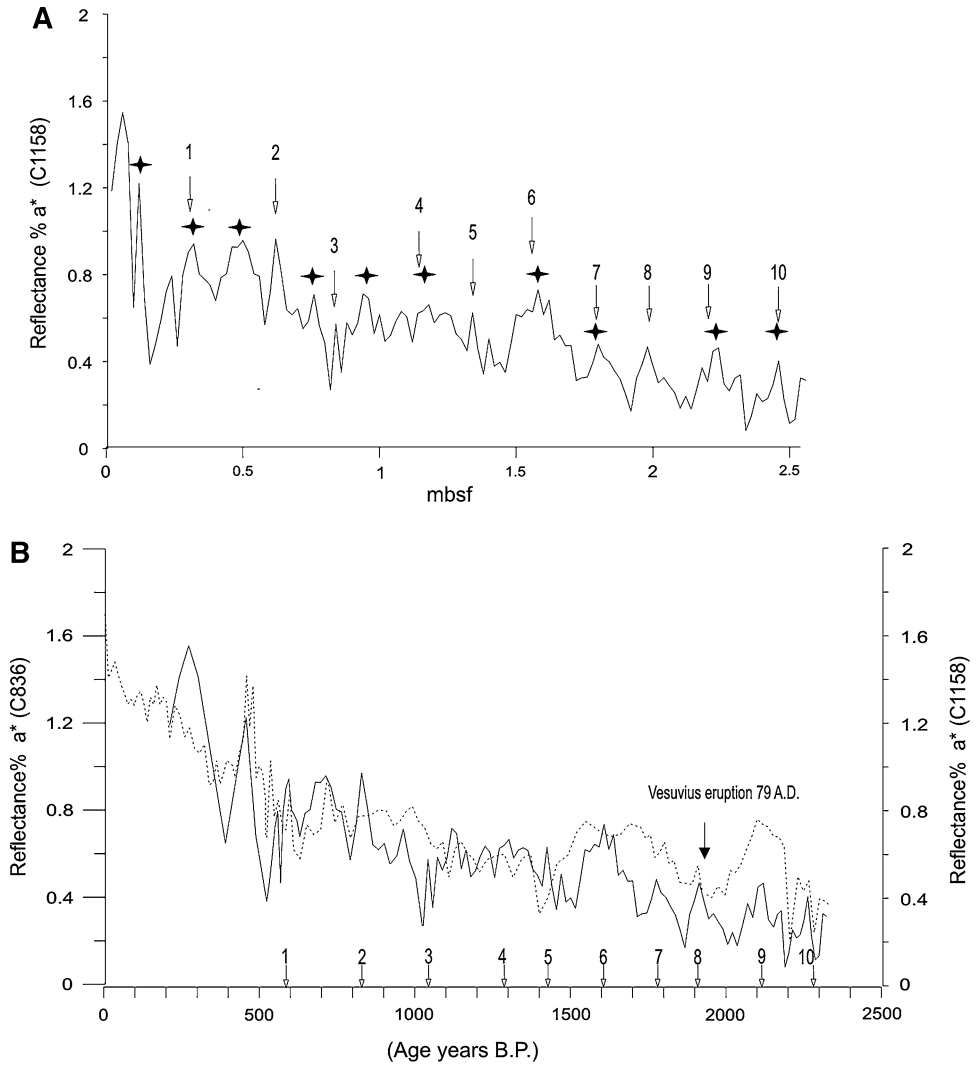

Fig. 8 Comparison in time domain of colour reflectance data for cores C1158 and C836. **a** Chromaticity reflectance data a* of core C1158 plotted versus depths (expressed in meter below sea floor). *Stars* indicate correlated distinctive directional swings present in both cores C1158 (This study) and C836 (Iorio et al. 2009) and utilized as tie points in the depth-age model. *Numbers and arrows* indicate the respective depths of the ten sedimentological-petrophysical correlated variations, occurring in core C1158 and C1162 (this study). **b** Comparison in time domain of chromaticity reflectance data a* of core C1158 (*black line*) with reflectance data a* for core C836 (*dot line*) (after Iorio et al. 2004a, 2009; Sacchi et al. 2009; Lirer et al. 2013) see text for details. *Numbers and arrows*, at the base of the graph, indicate the ages of the synchronous events (1–10), listed in Table 1, of petrophysical and sedimentological variations recognised in C1158 and C1162 cores. The *black arrow* indicates the interruption in the C836 a* record, due to the lack of a 1 m tephra bed deposited by Vesuvius during the Plinian eruption of Pompeii (AD 79), which was removed as an instantaneous event (Iorio et al. 2004a, 2009 and references therein)

is in agreement with the development of the Volturno delta front system, the formation of which started after the Holocene climatic optimum (5–7 kyr) (Buccheri et al. 2002; Amorosi et al. 2012).

5.2.2 Depositional processes

The extrapolated chronology for core C1158 also provides a precise age framework for our ten sedimentological petrophysical correlated peaks (Table 1) and suggests a regular change in the sediment supply processes. In fact, it is interesting to note that the average time interval among the ten correlated features is about 200 years. As we are in a sea level highstand, such sedimentological–petrophysical variations cannot be explained by sea level oscillation alone, and to date it has been accepted that there are no volcanic events in the Phlegraean Fields with similar frequencies. However, Allocca et al. (2000) stated that during the last 3,000 years the Campania region underwent several cold-humid, warm-arid climatic–environmental phases, which

Table 2 Chronology of silt or clay increasing layers

Increasing layers	A Silt/Clay	B Age (years BP)	C Time intervals among Silt or Clay increasing layers (years)
1	Silt	589	
2	Clay	830	241
3	Clay	830	212
4	Silt	1042	247
5	Clay	1429	140
6	Clay	1608	179
7	Silt	1780	172
8	Clay	1931	151
9	Clay	2115	184
10	Silt	2282	167
			Average 188 ± 37

A The ten correlated petrophysical-sedimentological silt or clay increasing layers. *B* Age occurrence of the ten increasing layers, based on the C836 and C1158 chromaticity parameter a* correlation. *C* Time intervals occurring between each pair of correlated layers. Average: mean value time and standard deviation

probably contributed to regular changes in the sediment supply. Moreover, if the preliminary estimate of about 200 years silt/clay variation time interval is confirmed, this value would fall in the well-known Suess cycle solar activity frequency (Suess 1980), and since solar forcing has a particularly strong impact on regional precipitation-evaporation budgets (e.g. Usoskin et al. 2004; Versteegh 2005), the regular changes in the sediment supply would be further supported.

5.2.3 Deformation processes

In the upper part of the HST unit (Figs. 2, 3) the interpretation of the origin and evolution of the observed subseafloor undulation features is not straightforward (Table 2).

At present, due to the important implications for offshore and coastal management, there is a quite vivid debate on the genetic mechanisms of these features. Their origin has been attributed to sediment deformation or depositional processes, also mixed theories were proposed (Urgeles et al. 2011 and references therein). Our observed features are similar to other examples where undulated reflectors characterize thick prodelta wedges on the Mediterranean shelves (e.g., Trincardi and Normark 1988; Correggiari et al. 2001; Lykousis et al. 2003). However, our undulated features, which appear to a depth of about −70 m, where the platform gradient starts to increase down to the abrupt change of the shelf break, are characterized by sediment with high water content, high sedimentation rate (1.1 mm/yr) and fluid escape features and show the presence of differently oriented extensional features (small-offset faults) equally distributed downslope, which extend to the same mean depth below seafloor.

So far a possible interpretation in the study area would consider the observed undulated reflectors as a metastable sediment load in a low-energy environment, and would relate such reflectors, characterized by small-offset faults, to shear-dominated failure, with limited downslope displacement, triggered by platform shelf gradient deepening and earthquakes, which are recurrent in a volcanic area as Phlegraean Fields.

An alternate option is considering these undulations as sediment waves produced by depositional processes, similar to the interpretations made in other middle size river prodelta areas interested by interplay of sedimentation and cyclonic bottom current along the shelf (e.g. Trincardi and Normark 1988) or for example by river-sourced storming events or hyperpycnal flows, (e.g. Urgeles et al. 2007, 2011 and references therein).

However, unlike most undulations produced by bottom water masses, our undulated features seem unrelated to erosional features, showing displaced reflectors produced by the sliding plain reaching the seafloor and do not show a downward displacement of reflectors along the shelf (Fig. 2 inset A and B) (Verdicchio and Trincardi 2006; Urgeles et al. 2011). Moreover, a different evidence in favour of a slow sliding with a limited downward displacement process may be furnished by the seismic interpretation, coupled with gravity core data, which highlight that this sector of the HST upper unit includes the same rich in water content mud layers and that such layers, being contemporaneously characterized by undisturbed sedimentation and preservation of the internal geometry, suggest a lack of reworking (Figs. 5, 7).

So far taking in account sediment characteristic and having excluded late Holocene hyperpycnal flows for the Volturno river, the influences of bottom current activity is considered a less likely hypothesis altogether subordinated to sediment deformation.

6 Conclusions

A multiproxy analysis of highstand deposits in a prodelta area, (Volturno River, Eastern Tyrrhenian Sea) was carried out to define sedimentary characteristics and processes. The seismostratigraphic analysis of the outer shelf in the studied area allowed to recognize a late Pleistocene wedge, topped by the post-Glacial Holocene ravinement surface, which constitutes a regional stratigraphic marker. Above such a surface, Holocene transgressive deposits occur while the Volturno prodelta deposits develop on the MFS.

Moreover, by means of correlations of colour chromaticity a* parameter of this study with a nearby high-resolution dated continental shelf record, a chronostratigraphic framework of the upper part of the prodelta highstand deposits was furnished and a time interpretation of about 2,300 years BP is provided. Further support to this age interpretation was provided by seismostratigraphic evidences and from the age of the development of the Volturno delta front system, the formation of which started after the Holocene climatic optimum (5–6 kyr).

In the sedimentological record of the upper unit of the prodelta highstand deposits, ten lithological-petrophysical correlated features were recognized. Based on the calculated depth–age conversion, an average time interval of ~ 200 years for the lithological correlated features was found; this time interval falls in the time range of the well-known solar activity frequency of Suess cycles. So far, as solar forcing seems to have a particularly strong impact on regional precipitation-evaporation budgets, it was possible to link the sedimentological variations found with regular climatic changes in the sediment supply. In addition, seismic profiles interpretation shows, in the study area, late Holocene highstand deposits, deposited in undisturbed sedimentation, which are interested by sediment undulations with a preserved internal geometry at decimetric scale. The preservation of internal geometry testifies a slow sliding without reworking. So far a possible recent (<2,300 years BP) shear dominated downward displacement related to high sediment supply, high water content and fluid escape features (pockmarks, seeps) and characterized by small-offset faults, located along gradient changes in the sea floor, with the occurrence of seismic activity representing a triggering factor, is inferred.

Finally for the first time, spectrophotometry correlations of Holocene shelf margins highstand deposits, several kilometres apart, have been detected, thus going beyond the previous work and confirming even for continental shelf areas the potential value of spectrophotometer data in high-resolution correlations.

Acknowledgments This research was supported by the Region Campania (CARG Project; Sector of Soil Defense, Via A. De Gasperi, 80133, Naples, Italy), Sannio University and National Research Council. The writers are particularly grateful to the crew of the Urania Vessel. The Petrophysical and Sedimentological analyses were performed at the IAMC-CNR Petrophysical Laboratory and at the Stratigraphic Laboratory of the Department of Geological and Enviromental Studies, Sannio University. The authors are grateful to two anonymous reviewers for valuable suggestions.

References

Aiello G, Marsella E, Sacchi M (2000) Quaternary structural evolution of the Terracina and Gaeta basins (Eastern Tyrrhenian margin, Italy). Rend Fis Acc Lincei 11:41–58

Aiello G, Cicchella AG, Di Fiore V, Marsella E (2011) New seismostratigraphic data of the Volturno Basin (northern Campania, Tyrrhenian margin, Southern Italy): implications for tectonostratigraphy of the Campania and Latium sedimentary basins. Ann Geophys 54(3):265–283

Allocca F, Amato V, Coppola D, Giaccio B, Ortolani F, Pagliuca S (2000) Cyclical climatic-environmental variations during the Holocene in Campania and Apulia: geoarcheological and paleoethnological evidences. Memorie Società Geologica Italiana 55:345–352

Amore FO, Ciampo G, Di Donato V, Esposito P, Pennetta M, Russo Ermolli E, Staiti D, Valente A (1996) A multidisciplinary study of Late Pleistocene-Holocene sediments of the Gaeta bay continental shelf. Il Quaternario 9(2):521–532

Amorosi A, Pacifico A, Rossi V, Ruberti D (2012) Late Quaternary incision and deposition in an active volcanic setting: The Volturno valley fill, southern Italy. Sed Geol 282:307–320

Aucelli PPC, Amato V, Budillon F, Senatore MR, Amodio S, D'Amico C, Da Prato S, Ferraro L, Pappone G, Russo Ermolli E (2012) Evolution of the Sele River coastal plain (southern Italy) during the Late Quaternary by inland and offshore stratigraphical analyses. Rend Fis Acc Lincei 23(1):81–102. doi:10.1007/s12210-012-0165-5

Balsam WL, Beeson JP (2003) Sea-floor sediment distribution in the Gulf of Mexico. Deep-Sea Research, Part 1. Oceanogr Res Papers 12:1421–1444

Balsam WL, Damuth JE (2000) Further investigations of shipboard VS shore-based spectral data: Implications for interpreting Leg 164 sediment composition. In: Paull CK, Matsumoto R, Wallace PJ, Dillon WP (eds) Proceedings ODP, Scientific Results, 164. pp 313–324

Balsam WL, Deaton BC (1991) Sediment dispersal in the Atlantic Ocean: evaluation by visible spectra. Rev Aquat Sci 4:411–447

Balsam WL, Deaton BC (1996) Determining the composition of Late Quaternary marine sediments from NUV, VIS, and NIR diffuse reflectance spectra. Mar Geol 134(1–2):31–55

Balsam WL, Wolhart R (1993) Sediment dispersal in the Argentine Basin: evidence from visible light spectra. Deep Sea Res 40:1001–1031

Balsam WL, Damuth JE, Schneider RR (1997) Comparison of Shipboard vs Shore-Based Spectral Data from Amazon Fan Cores: Implications for Interpreting Sediment Composition. In: Flood RD, Piper DJW, Klaus A, Peterson LC (eds) Proceedings ODP, Scientific Results, 155. pp 193–215

Balsam WL, Deaton BC, Damuth JE (1999) Evaluating optical lightness as a proxy for carbonate content in marine sediment cores. Mar Geol 161:141–153

Balsam WL, Damuth JE, Deaton BC (2007) Marine sediment components: identification and dispersal assessed by diffuse reflectance spectrophotometry. Int J Environ Health 1(3): 403–426

Barra D, Romano P, Santo A, Campajola L, Roca V, Tuniz C (1996) The versilian transgression in the Volturno river plain: palaeoenvironmental history and chronological data. Il Quaternario 10:571–578

Barranco FT, Balsam WL, Deaton BC (1989) Quantitative reassessment of brick red lutites: Evidence from reflectance spectrophotometry. Mar Geol 89:299–314

Bartole R, Savelli D, Tramontana M, Wezel FC (1984) Structural and sedimentary features in the Tyrrhenian margin off Campania, Southern Italy. Mar Geol 55:163–180

Belloni S (1969) Una tabella universale per eseguire granulometrie col metodo della sedimentazione unica o col metodo del densimetro di Casagrande modificato. Geologia Tecnica 16:1281–1289

Bellotti P (2000) Il modello morfo-sedimentario dei maggiori delta tirrenici italiani. Bollettino della Società Geologica Italiana 119:777–792

Bruno PP, Di Fiore V, Ventura G (2000) Seismic study of the '41st Parallel' Fault System offshore the Campanian-Latial continental margin. Italy Tectonophys 324(1–2):37–55

Buccheri G, Capretto G, Di Donato V, Esposito P, Ferruzza G, Pescatore T, Russo Ermolli E, Senatore MR, Sprovieri M, Bertoldo M, Carella D, Madonia G (2002) A high resolution record of the last deglaciation in the southern Tyrrhenian Sea: environmental and climatic evolution. Mar Geol 186:447–470

Budillon F, Violante C, Conforti A, Esposito E, Insinga D, Iorio M, Porfido S (2005) Event beds in the recent prodelta stratigraphic record of the small flood-prone Bonea Stream (Amalfi Coast, Southern Italy). Mar Geol 222–223:419–441

Budillon F, Lirer F, Iorio M, Macri P, Sagnotti L, Vallefuoco M, Ferraro L, Garziglia S, Innangi S, Sahabi M, Tonielli R (2009) Integrated stratigraphic reconstruction for the last 80 kyr in a deep sector of the Sardinia Channel (Western Mediterranean). Deep Sea Res II 56:725–737

Budillon F, Senatore MR, Insinga DD, Iorio M, Lubritto C, Roca M, Rumolo P (2012) Late Holocene sedimentary changes in shallow water settings: the case of the Sele river offshore in the Salerno Gulf (south-eastern Tyrrhenian Sea, Italy). Rend Fis Acc Lincei 23(1):25–43. doi:10.1007/s12210-012-0164-6

Casciello E, Cesarano M, Pappone G (2006) Extensional detachment faulting on the Tyrrhenian margin of the southern Apennines contractional belt (Italy). J Geol Soc London 163:617–629

Cattaneo A, Correggiati A, Marsset T, Yannick T, Marsset B, Trincardi F (2004) Seafloor undulation pattern on the Adriatic shelf and comparison to deep-water sediments waves. Mar Geol 213:121–148

Catuneanu O, Abreu V, Bhattacharya JP, Blum MD, Dalrymple RW, Eriksson PG, Fielding CR, Fischer WL, Galloway WE, Gibling MR, Giles KA, Holbrook JM, Jordan R, Kendall CGStC, Macurda B, Martinsen OJ, Miall AD, Neal JE, Nummedal D, Pomar L, Posamentier HW, Pratt BR, Sarg JF, Shanley KW, Steel RJ, Strasser A, Tucker ME, Winker C (2009) Towards the standardization of sequence stratigraphy. Earth Sci Rev 92(1–2):1–33

Chappell J, Shackleton NJ (1986) Oxygen isotopes and sea level. Nature 324:137–140

Chiocci FL (1994) Very High-Resolution seismics as a tool for sequence stratigraphy applied to outcrop scale. Examples from eastern Tyrrhenian margin Holocene/Pleistocene deposits. Am Assoc Pet Geol Bull 78:378–395

Chiocci FL, Casalbore D (2011) Submarine gullies on Italian upper slopes and their relationship with volcanic activity revisited 20 years after Bill Normark's pioneering work. Geosphere 7(6):1–11. doi:10.1130/GES00633

Chiocci FL, Ercilla G, Torres J (1997) Stratal architecture of Western Mediterranean margins as the result of the stacking of Quaternary lowstand deposits below glacio-eustatic fluctuation base-leve. Sed Geol 112:195–217

Christian HA, Mosher DC, Mulder T, Barrie JV, Courtney RC (1997) Geomorphology and potential slope instability on the Fraser River delta foreslope, Vancouver, British Columbia. Can Geotech J 34(3):432–446. doi:10.1139/t97-007

Ciampo G (2003) Reconstruction of late pleistocene—Holocene palaeobathymetries from Ostracoda on the Tyrrhenian continental shelf. Geobios 36:1–11

CIE, Commission Internationale de l'Eclairage (1978) Recommendations on Uniform Color Space, Color-Difference Equations and Psychometric color Terms, Supplement No. 2 Publication CIE No. 15 (E-1.3.1)/(TC-1.3), Paris: Bureau Central de la CIE

Cocco E, De Pippo T (1988) Tendenze evolutive delle spiagge della Campania e della Lucania. Memorie della Società Geologica Italiana 41:195–204

Cocco E, De Pippo T, Massari P (1988) L'uso delle sabbie fluorescenti per la valutazione del drift litoranee lungo il litorale domitio (Golfo di Gaeta). Memorie della Società Geologica Italiana 41:869–876

Coleman JM (1988) Dynamic changes and processes in the Mississippi River Delta. Geol Soc Am Bull 100:999–1015

Coppa MG, Ferraro L, Pennetta M, Russo B, Valente A, Secchione C (1996) Sedimentology and micropaleontology of the core G39-C27 (Gaeta bay, central Tyrrhenian Sea, Italy). Il Quaternario 9(2):687–696

Correggiari A, Trincardi F, Langone L, Roveri M (2001) Styles of failure in late Holocene highstand prodelta wedges on the Adriatic shelf. J Sediment Res 71:218–236

D'Argenio A, Pescatore T, Senatore MR (2004) Sea-level change and volcano-tectonic interplay. The Gulf of Pozzuoli (Campi Flegrei, Eastern Tyrrhenian Sea) during the last 39 ka. J Volcanol Geoth Res 133:105–121

Dalrymple RW, Zaitlin BA, Boyd R (1992) Estuarine facies models: conceptual basin and stratigraphic implications. J Sediment Petrol 62:1130–1146

De Pippo T, Donadio C, Pennetta M (2004) Morphological control on sediment dispersal along. The Southern Tyrrhenian coastal zones (Italy). Geol Romana 37:113–121

De Pippo T, Donadio C, Pennetta M, Petrosino C, Terlizzi F, Valente A (2008) Coastal hazard assessment and mapping in Northern Campania, Italy. Geomorphology 97:451–466

De Vita S, Orsi G, Civetta L, Carandente A, D'Antonio M, Deino A, di Cesare T, Fisher RV, Isaia R, Marotta E, Necco A, Ort MH, Pappalardo L, Piochi M, Southon J (1999) The Agnano-Monte Spina eruption (4100 years BP) in the restless Campi Flegrei-icaldera. J Volcanol Geotherm Res 91:269–301

De Vivo B, Rolandi G, Gans PB, Calvert A, Bohrson WA, Spera FJ, Belkin HE (2001) New constraints on the pyroclastic eruptive history of the Campanian volcanic Plain (Italy). Mineral Petrol 73:47–65

Deaton BC, Balsam WL (1991) Visible spectroscopy-a rapid method for determining hematite and goethite concentration in geological materials. J Sediment Petrol 61:628–632

Debret M, Desmet M, Balsam W, Copard Y, Francus P, Laj C (2006) Spectrophotometer analysis of Holocene sediments from an anoxic fjord: Saanich Inlet, British Columbia, Canada. Mar Geol 229:15–28

Deino AL, Orsi G, Piochi M, De Vita S (2004) The age of the Neapolitan yellow Tuff caldera-forming eruption (Campi Flegrei caldera—Italy) assessed by 40Ar/39Ar dating method. J Volcanol Geoth Res 133:157–170

Di Vito MA, Isaia R, Orsi G, Southon J, De Vita S, D'Antonio M, Pappalardo L, Piochi M (1999) Volcanism and deformation in thepast 12 ka at the Campi Flegrei caldera (Italy). J Volcanol-Geotherm Res 91:221–246

Duke W (1985) Hummocky cross-stratification, tropical hurricanes and intense winter storms. Sedimentology 32:167–194

Duke W (1990) Geostrophic circulation or shallow marine turbidity currents? The dilemma of paleoflow patterns in storm influenced prograding shoreline systems. J Sediment Petrol 60:870–883

Einsele G (2000) Sedimentary Basin: evolution, facies and sedimentary budget. Springer, Berlin, p 792

Florio G, Fedi M, Cella F, Rapolla A (1999) The campanian plain and Phlegraean fields: structural setting from potential field data. J Volcanol Geoth Res 91:361–379

Folk RL (1965) Petrology of sedimentary rocks. Hemphill's Drawer M, University Station

Folk RL, Ward WC (1957) Brazos river bar: a study in the significance of grain size parameters. J Sediment Petrol 27:3–26

Gaffey S (1985) Reflectance spectroscopy in the visible and near-infrared (0.35–2.55 micron): applications in carbonate petrology. Geology 13:270–273

Giosan L, Flood RD, Aller RC (2002) Paleoceanographic significance of sediment color on western North Atlantic drifts: I. Origin of color. Mar Geol 189:25–41

Hagelberg T, Shackleton MJ, Pisias N and Shipboard Scient. Party (1992) Development of composite depth sections for Sites 844 trough 854. In: Mayer LA, Pisias NG, Janecek TR et al. (eds) Proceedings ODP Initial Reports, ODP, Texas, USA, A&M University, pp 79–85

Helmke JP, Shulz M, Bauch H (2002) Sediment-Color record from the Northeast Atlantic reveals patterns of Millennial-Scale Climate Variability during the past 500,000 years. Quatern Res 57(1):49–57

Herbert TD, Tom BA, Burnett C (1992) Precise major component determinations in deep-sea sediments using Fournier transform infrared spectroscopy. Geochim Cosmochim Acta 56:1759–1763

Hunt D, Tucker ME (1992) Stranded parasequence and the forced regressive wedge systems track: deposition during base-level fall. Sed Geol 181:1–9

Iorio M, Sagnotti L, Angelino A, Budillon F, D'Argenio B, Dinarès-Turell J, Macrì P, Marsella E (2004a) High resolution petrophysical and palaeomagnetic study of Late Holocene shelf sediments, Salerno Gulf, Tyrrhenian Sea. Holocene 14(3):426–435

Iorio M, Wolf-Welling T, Moerz T (2004b) Antarctic sediment drifts and Plio-Pleistocene orbital periodicities (ODP Sites 1095, 1096, and 1101). In: D'Argenio B, Fischer AG, Premoli Silva I, Weissert H, Ferreri V (eds) Cyclostratigraphy: an essay of approaches and case histories. Society for Sedimentary Geology, SEPM, Special Publication 81:231–244

Iorio M, Liddicoat J, Budillon F, Tiano P, Incoronato A, Coe R, Marsella E (2009) Palaeomagnetic secular variation time constrain on late neogene geological events in slope sediment from the Eastern Tyrrhenian Sea. In: Kneller B, Martinsen OJ, McCaffrey B (eds) External controls on deep-water depositional systems. Society for Sedimentary Geology, SEPM, Special Publication 92:233–243

Iorio M, Liddicoat J, Budillon F, Incoronato A, Coe RS, Insinga DD, Cassata WS, Lubritto C, Angelino A, Tamburrino S (2014) Combined palaeomagnetic secular variation and petrophysical records totime-constrain geological and hazardous events: An example from the eastern Tyrrhenian Sea over the last 120 ka. Global Planet Change 113:91–109

Lirer F, Sprovieri M, Ferraro L, Vallefuoco M, Capotondi L, Cascella A, Petrosino P, Insinga DD, Pelosi N, Tamburrino S, Lubritto C (2013) Integrated stratigraphy for the Late Quaternary in the eastern Tyrrhenian Sea. Quatern Int 292:71–85

Lourens LJ (2004) Revised tuning of Ocean Drilling Program Site 964 and KC01B (Mediterranean) and implication for the δ18O, tephra, calcareous nannofossil, and geomagnetic reversal chronologies of the past 1.1 Myr. Paleocenography 19:PA3010. doi:10.1029/2003PA000997

Lykousis V, Sakellariou D, Rousakis G (2003) Prodelta slope stability and associated coastal hazards in tectonically active margins: Gulf of Corinth (NE Mediterranean). In: Locat J, Meinert J (eds) Submarine mass movements and their consequences. Kluwer Academic Press, Dordrecht, The Netherlands, pp 433–440

Lykousis V, Roussakis G, Sakellariou D (2009) Slope failures and stability analysis of shallow water prodeltas in the active margins of Western Greece, northeastern Mediterranean Sea. Int J Earth Sci (Geol Rundsch) 98:807–822

Malinverno A, Ryan WBF (1986) Extension in the Tyrrhenian Sea and shortening in the Apennines as a result of arc migration driven by sinking of the lithosphere. Tectonics 5:227–245

Marani M, Taviani M, Trincardi F, Argnani A, Borsetti AM, Zitellini N (1986) Pleistocene progradation and post-glacial events of the NE Tyrrhenian continental shelf between the Tiber river delta and Capo Circeo. Memorie Società Geologica Italiana 36:67–89

Mariani M, Prato R (1988) I bacini neogenici costieri del margine tirrenico: approccio sismico-stratigrafico. Memorie Società Geologica Italiana 41:519–531

Miao X, Mason J, Johnson W, Wang H (2007) High-resolution proxy record of Holocene climate from a loess section in Southwestern Nebraska, USA. Palaeogeogr Palaeoclimatol Palaeoecol 245:368–381

Milia A, Torrente MM, Russo M, Zuppetta A (2003) Late-Quaternary volcanism and transtensional tectonics in the bay of Naples, Campanian continental margin, Italy. Mineral Petrol 79:49–65

Mix AC, Harris SE, Janecek T (1995) Estimating lithology from nonintrusive reflectance spectra: Leg 138. Proc ODP Sci Results 138:413–427

Moros M, Endler R, Lackschewitz KS, Wallrabe-Adams HJ, Mienert J, Lemke W (1997) Physical properties of Reykjanes Ridge sediments and their linkage to high-resolution Greenland Ice Sheet project 2 ice core data. Paleoceanography 12:687–695

Mudler T, Syvitski JPM (1995) Turbidity currents generated at river mouths during exceptional discharges to the world oceans. J Geol 103:285–299

Nagao S, Nakashima S (1992) The factors controlling vertical colour variations of North Atlantic Madeira abyssal plain sediments. Mar Geol 109:83–94

Nichol SL, Boyd R, Penland S (1996) Sequence stratigraphy of a coastal-plain incised valley estuary: Lake Calcasieu, Louisiana. J Sediment Res 66:847–857

Orsi G, Di Vito MA, Isaia R (2004) Volcanic hazard assessment at the restless Campi Flegrei caldera. Bull Volcanol 66:514–530

Ortiz JD, Rack FR (1999) Non-invasive sediment monitoring methods: current and future tools for high-resolution climate studies. In: Abrantes F, Mix A (eds) Reconstructing ocean history: a window to the future. Kluwer Academic/Plenum Publishers, New York, pp 343–380

Ortiz J, Mix A, Harris S, O'Connell S (1999) Diffuse spectral reflectance as a proxy for percent carbonate content in North Atlantic sediments. Paleoceanography 14:171–186

Orton GJ, Reading HG (1993) Variability of deltaic process in terms of sediment supply, with particular emphasis on grain size. Sedimentology 40:475–512

Passega R (1957) Texture as characteristic of clastic deposition. Am Assoc Pet Geol Bull 41(9):1952–1984

Passega R (1964) Grain size representation by CM patterns as a geological tool. J Sediment Petrol 34(4):830–847

Passega R (1977) Significance of CM diagram of sediment deposited by suspension. Sedimentology 24:23–33

Pennetta M, Valente A, Abate D, Budillon G, De Pippo T, Leone M, Terlizzi F (1998) Influenza della morfologia costiera sulla circolazione e sedimentazione sulla piattaforma continentale campano-laziale tra Gaeta e Cuma (Italia meridionale). Boll Soc Geol Ital 117:281–295

Petruccione E, Aiello G, Capretto G, Senatore M R, Marsella E, Iorio M (2011) Holocene Sedimentary and Gravitative Processes in Highstand Prodelta Deposits on the Cuma outer shelf (Eastern Tyrrhenian sea, Italy): An Integrated Approach "Marine Research at CNR", Volume Mare—CNR Dipartimento Terra e Ambiente, DTA, 771–784

Porebski SJ, Steel RJ (2003) Shelf-margin deltas: their stratigraphic significance and relation to deepwater sands. Earth Sci Rev 62:283–326

Posamentier HW, Allen GP, James DP, Tesson M (1992) Forced regressions in a sequence stratigraphic framework: concepts, examples, and exploration significance. Am Assoc Pet Geol Bull 76:1687–1709

Reading HG (1996) Sedimentary environments: processes, facies and stratigraphy. Blackwell Science, Oxford, p 688

Robinson SG, Maslin MA, McCave IN (1995) Magnetic susceptibility variability in Upper Pleistocene deep-sea sediments of the NE Atlantic: implications for ice rafting and paleocirculation at the last glacial maximum. Paleoceanography 10:221–250

Romano P, Santo A, Voltaggio M (1994) L'evoluzione geomorfologia della Pianura del Fiume Volturno (Campania) durante il Tardo Quaternario (Pleistocene medio-superiore-Olocene). Il Quaternario 7(1):41–56

Sacchi M, Insinga D, Milia A, Molosso F, Raspini A, Torrente M, Conforti A (2005) Stratigraphic signature of the Vesuvius 79 AD event off the Sarno prodelta system, Naples Bay. Mar Geol 222–223:443–469

Sacchi M, Molisso F, Violante C, Esposito E, Insinga D, Lubritto C, Porfido S, Tóth T (2009) Sea seismic examples off the Amalfi cliffed coasts, eastern Tyrrhenian. Insights into flood-dominated fan-deltas: very high-resolution. In: Violante C (ed) Geohazard in Rocky Coastal Areas. Geological Society, Special Publications, London, 322:33–71

Sagnotti L, Budillon F, Dinare'S-Turell J, Iorio M, Macrì P (2005) Evidence for a variable paleomagnetic lock-in depth in the Holocene sequence from the Salerno Gulf (Italy): Implications for high-resolution paleomagnetic dating. Geochemestry Geophysics Geosystem 6:Q11013. doi:10.1029/2005GC001043

Scandone R, Bellucci F, Lirer L, Rolandi G (1991) The structure of the Campanian Plain and the activity of the Neapolitain volcanoes (Italy). J Volcanol Geoth Res 48:1–31

Shepard FP (1954) Nomenclature based on sand–silt–clay ratios. J Sediment Petrol 24(3):151–158

Suess HE (1980) The radiocarbon record in tree rings of the last 8000 years. Radiocarbon 22:200–209

Suter JR, Berryhill HL Jr (1985) Late Quaternary shelf-margin deltas, northwest Gulf of Mexico. AAPG Bull 69:77–91

Swift DJP, Phillips S, Thorne JA (1991) Sedimentation on continental margins, IV: Lithofacies and depositional systems. In: Swift DJP, Oertel GF, Tillman RW, Thorne JA (eds) Shelf sand and sandstone bodies: geometries, facies and sequence stratigraphy. International Association of Sedimentologists, Special Publication 14:89–152

Torrente MM, Milia A (2013) Volcanism and faulting of the Campania margin (Eastern Tyrrhenian Sea, Italy): a three-dimensional visualization of a new volcanic field off Campi Flegrei. Bull Volcanol 75:719. doi:10.1007/s00445-013-0719-0

Trincardi F, Field ME (1991) Geometry, lateral variation, and preservation of downlapping regressive shelf deposits: eastern Tyrrhenian Sea margin, Italy. J Sediment Petrol 6(5):775–790

Trincardi F, Normark WR (1988) Sediment waves on the Tiber prodelta slope. Geo-Mar Lett 8:149–157

Trincardi F, Cattaneo A, Correggiati A, Ridente D (2004) Evidence of soft sediment deformation, fluid escape, sediment failure and regional weak layers within the late Quaternary mud deposits of the Adriatic Sea. Mar Geol 213:91–119

Tucker M (1988) Techniques in sedimentology. Blackwell Scientific Publications, Oxford, p 394

Urgeles R, DeMol B, Liquete C, Canals M, De Batist M, Hughes-Clarke JE, Amblas D, Arnau PA, Calafat AM, Casamor JL, Centella V, De Rycker K, Fabres J, Frigola J, Lafuerza S, Lastras G, Sanchez A, Zuniga D, Versteeg W, Willmott V (2007) Sediments undulations on the Llobregat prodelta: Signs of early slope instability or sedimentary bedforms? J Geophys Res 112:B05102. doi:10.1029/2005JB003929

Urgeles R, Cattaneo A, Puig P, Liquete C, De Mol B, Amblas D, Sultan N, Trincardi F (2011) A review of undulated sediment features on Mediterranean prodeltas: distinguishing sediment transport structures from sediment deformation. Marine Geophys Res 32:49–69

Usoskin IG, Mursula K, Solanki S, Schùssler M, Alanko K (2004) Reconstruction of solar activity for the last millennium using 10 Be data. Astron Astrophys 413:745–751

Vail PR, Mitchum RM, Thompson III S (1977) Seismic stratigraphy and global changes of sea level. In: Payton CE (ed) Seismic stratigraphy-applications to hydrocarbon exploration. American Association of Petroleum Geologists Memoir, 26:49–212

Vail PR, Audemard F, Bowman SA, Eisner PN, Perez-Cruz G (1991) The stratigraphic signatures of tectonics, eustasy and sedimentation: an overview. In: Seilacher A, Eisner G (eds) Cycles and Events in Stratigraphy, II. Springer, Tubingen, pp 617–659

Vallefuoco M, Lirer F, Ferraro L, Pelosi N, Capotondi L, Sprovieri M, Incarbona A (2012) Climatic variability and anthropogenic signatures in the Gulf of Salerno (southern–eastern Tyrrhenian Sea) during the last half millennium. Rend Fis Acc Lincei 23:13–23. doi:10.1007/s12210-011-0154-0

Van Wagoner JC, Posamienter HW, Mitchum RM, Vail PR, Sarg JF, Loutit TS, Hardenbol J (1988) An overview of the fundamentals of sequence stratigraphy and key definitions. Sea-Level Changes. An Integrated Approach. Society for Sedimentary Geology, SEPM Special Publication, 42:40–45

Verdicchio G, Trincardi F (2006) Short-distance variability in slope bed-forms along the southwestern Adriatic margin (central Mediterranean). Mar Geol 234:271–292

Versteegh GJM (2005) Solar forcing of climate. 2: evidence from the past. Space Sci Rev 120:243–286

Weber ME, Niessen F, Kuhn G, Wiedicke M (1997) Calibration and application of marine sedimentary properties using a multi-sensor core logger. Mar Geol 136:51–172

Wolf-Welling TCW, Cowan EA, Daniels J, Eyles N, Maldonado A, Pudsey CJ (2001) Data report: Diffuse spectral reflectance data from rise Sites 1095, 1096, and 1101 and Palmer Deep Sites 1098 and 1099 (Leg 178, western Antarctic Peninsula). In: Barker PF, Camerlenghi A, Acton GD, Ramsay ATS (eds) Proceedings ODP, Scientific Results, 178:1–22

Wright LD (1977) Sediment transport and deposition at river mouth: a synthesis. Geol Soc Am Bull 88:857–868

Wright LD, Chappell J, Thom BG, Bradshaw MP, Cowell P (1979) Morphodynamics of reflective and dissipative beach and inshore systems: Southeastern Australia. Mar Geol 32:105–140

Wright LD, Wiseman WJ, Bornhold BD, Suhayda JN, Keller GH, Yang ZS, Fan YB (1988) Marine dispersal and deposition of Yellow River silt by gravity-driven underflows. Nature 332:629–632

Zecchin M, Catuneanu O (2013) High-resolution sequence stratigraphy of clastic shelves I: Units and bounding surfaces. Mar Pet Geol 39:1–25